AGU ADVANCING EARTH AND SPACE SCIENCES

Geophysical Research Letters

RESEARCH LETTER
10.1029/2025GL117217

Permeability Evolution and Gouge Formation During Fracture Shearing

Marco Fuchs[1], Philipp Blum[1], Guido Blöcher[2,3], and Luc Scholtès[4]

[1]Institute of Applied Geosciences (AGW), Karlsruhe Institute of Technology (KIT), Karlsruhe, Germany, [2]GFZ Helmholtz Centre for Geosciences, Potsdam, Germany, [3]Department of Engineering Geology, TU Berlin, Berlin, Germany, [4]Université Clermont Auvergne, CNRS, IRD, OPGC, Laboratoire Magmas et Volcans, Clermont-Ferrand, France

Abstract Hydro-mechanical processes are crucial in shear-controlled geoscientific applications such as enhanced geothermal systems and often result in stress-dependent permeability changes. The present study aims to investigate shear-induced permeability evolution of a natural sandstone fracture using a novel modeling approach. Combining a mechanical discrete element model and a hydraulic finite element model, three normal stress-related hydro-mechanical regimes can be identified. Under low normal stress conditions (<4.0 MPa), permeability is enhanced during shearing due to dilation on intact asperities. With increasing normal stress, asperities break and gouge is formed, leading to a normal stress-related transition where permeability tends to decrease during shearing. In our study, this transition occurs when normal stress equals the rock's ultimate tensile strength (4.0 MPa). For normal stresses >4.0 MPa, permeability decreases during shearing due to intense fracture surface damage.

Plain Language Summary Being able to characterize fracture flow in the subsurface is essential to sustainably manage geothermal reservoirs. Previous studies have shown that fracture permeability can either increase or decrease when fractures are sheared. Using computer simulations, we studied how the normal stress influences permeability changes of a single sandstone fracture subjected to shearing. Our results highlight three different regimes depending on the normal stress applied to the fracture. At low normal stress, the fracture asperities remain intact during shearing and favor fracture opening which induces an overall increase of the permeability. At high normal stresses, the asperities break during shearing and favor fracture closing which produce a decrease of the permeability. For intermediate normal stresses, a transitional regime is observed, in which permeability remains constant during shearing.

Key Points:

- Hydraulic opening occurs under low normal stresses and is governed by dilation on intact asperities
- The transition between shear induced hydraulic opening and closing of rock fractures is normal stress-dependent
- Hydraulic closing occurs under high normal stresses and is related to fracture surface damage and gouge formation

Supporting Information:

Supporting Information may be found in the online version of this article.

Correspondence to:

M. Fuchs,
marco.fuchs@kit.edu

Citation:

Fuchs, M., Blum, P., Blöcher, G., & Scholtès, L. (2025). Permeability evolution and gouge formation during fracture shearing. *Geophysical Research Letters*, *52*, e2025GL117217. https://doi.org/10.1029/2025GL117217

Received 3 JUN 2025
Accepted 2 NOV 2025

Author Contributions:

Conceptualization: Marco Fuchs, Philipp Blum, Luc Scholtès
Investigation: Marco Fuchs, Guido Blöcher
Methodology: Marco Fuchs, Luc Scholtès
Software: Marco Fuchs, Luc Scholtès
Supervision: Philipp Blum, Guido Blöcher, Luc Scholtès
Validation: Marco Fuchs, Guido Blöcher, Luc Scholtès
Visualization: Marco Fuchs
Writing – original draft: Marco Fuchs, Luc Scholtès
Writing – review & editing: Marco Fuchs, Philipp Blum, Guido Blöcher, Luc Scholtès

1. Introduction

Understanding the hydro-mechanical (HM) behavior of fractures is essential for subsurface systems such as enhanced geothermal systems (EGS) where hydraulic stimulation plays a crucial role (Amann et al., 2018). Hydraulic stimulation increases fluid pressures that reduce the effective stress and potentially enable shear slips of existing fractures (e.g., Ellsworth, 2013; Nguyen et al., 2021), which, in turn, induce permeability changes that can have drastic effects at the reservoir scale.

Empirical models can be used to correlate permeability and geometrical properties of single fractures. One fundamental model is the cubic law that relates permeability and mechanical aperture (Louis, 1969; Witherspoon et al., 1980). Since the cubic law was developed for two parallel plates, other studies tried to enhance its capability by including additional parameters in its formulation such as relative roughness (e.g., Barton & De Quadros, 1997; Renshaw, 1995), joint roughness coefficient (e.g., Barton, 1982; Olsson & Barton, 2001), or contact area (e.g., Walsh, 1981; Zimmerman & Bodvarsson, 1996). However, most of these existing models do not consider shear-related processes, such as dilation on asperities, or gouge and contact area formation (Cardona et al., 2021).

HM coupled direct shear tests (DST) are commonly used to investigate fracture permeability evolution during shearing (e.g., Frash et al., 2016; Li et al., 2023). Based on such tests, two shear-induced hydraulic regimes have been identified: (a) an opening regime associated with a permeability increase, and (b) a closing regime associated with a permeability decrease. These regimes are dependent on multiple factors, such as normal stress, surface roughness, and material properties (Fang and Wu, 2022). High-strength materials, low normal stresses, and pronounced surface roughness promote fracture opening (Fang and Wu, 2022). Thus, permeabilities of fractures

in granites or marbles tend to increase during shearing (Esaki et al., 1999; Wenning et al., 2019), whereas they tend to decrease in shales (Carey et al., 2015; Fang et al., 2017), although exceptions exist (Frash et al., 2016; Li et al., 2023).

Since DST are destructive for the tested fractures, systematic studies on natural fractures are challenging. Thus, many studies have used artificial fractures (e.g., saw-cut fractures, 3D printed fractures), which, however, have only limited significance due to their specific morphology and material properties (Fang and Wu, 2022; Tatone & Grasselli, 2015). Alternatively, numerical approaches provide a relevant alternative to study such HM-coupled and progressive processes due to their flexibility and evolving capabilities. However, studies providing 3D HM coupled models to investigate permeability changes during shearing remain scarce. Most numerical studies focus either on hydraulic flow and permeability changes during shearing or on mechanical processes, such as gouge or contact area formation (e.g., Chen et al., 2021; Wang et al., 2020). Hydraulic studies have been mostly performed using continuum approaches such as the finite element method (FEM) (e.g., Auradou, 2009; Matsuki et al., 1999) and thus tend to simplify or neglect mechanical processes such as gouge formation or fracture surface evolution, since they are not able to reflect breakages of asperities.

For an advanced representation of the mechanical behavior of fractures, discontinuum approaches, such as the discrete element method (DEM), have been increasingly used due to their capacity to describe explicitly progressive failure processes. DEM models can actually simulate the evolution of fracture contact area (Lambert & Coll, 2014) or the formation of gouge material (Asadi et al., 2012; Liu et al., 2016; Wang et al., 2019, 2020). However, due to the complex representation of fluid flow in DEM models, hydraulic processes are often neglected, and permeability changes are generally determined empirically (Wang et al., 2020).

In recent years, several studies focused on detailed investigations of permeability changes related to HM processes (Chen et al., 2021; Deng et al., 2024). For instance, Li et al. (2024) developed an approach that allows a mechanical DEM model to be coupled to a hydraulic FEM simulator in order to compute permeability changes during a DST simulation. Nonetheless, although technically possible, none of these studies focused on the effect of the normal stress on shear induced permeability changes.

Hence, the objective of this study is to investigate permeability changes of a natural sandstone fracture during shearing, considering specifically the influence of the normal stress on its evolution, using numerical experiments combining a mechanical DEM model and a hydraulic FEM model.

2. Materials and Methods

2.1. Fracture Sample

This study is built upon a natural bedding joint in a block of Flechtinger sandstone taken from a quarry in Bebertal, Germany (Fischer et al., 2012). Flechtinger sandstone is an oil and gas reservoir rock in the North German Basin considered for the development of EGS systems in recent years (Zimmermann et al., 2010). Thus, many previous studies investigated important HM parameters of the rock and its fractures, such as porosity, fracture and matrix permeability, fracture roughness, and grain size distribution (Blöcher et al., 2019; Cheng et al., 2020; Gutjahr et al., 2022; Hale & Blum, 2022; Hale et al., 2020; Hassanzadegan et al., 2012; Heidsiek et al., 2020; Heiland, 2003; Kluge et al., 2021). Due to the tectonic and diagenetic processes (Heidsiek et al., 2020) and superficial weathering, the fracture exhibits a low initial contact area (c.f., Text S3 in Supporting Information S1).

In this study, two representative, self-affine 3D point clouds of high-resolution surface scans of the bedding joint were used (Fuchs, Hale, et al., 2024; Gutjahr et al., 2022). The extent of the bedding joint as well as the extent of the scans is 450 mm in x-direction and 120 mm in y-direction. The average resolution of these scans is 250 µm (Fuchs, Hale, et al., 2024). Due to computational constraints, the scans were cropped to a section of 50 mm × 50 mm taken from the center of the point cloud (Figure 1). To facilitate its numerical handling, the irregular point clouds were assigned to a regular grid and matched spatially (Fuchs, Hale, et al., 2024; Fuchs, Suzuki, et al., 2024).

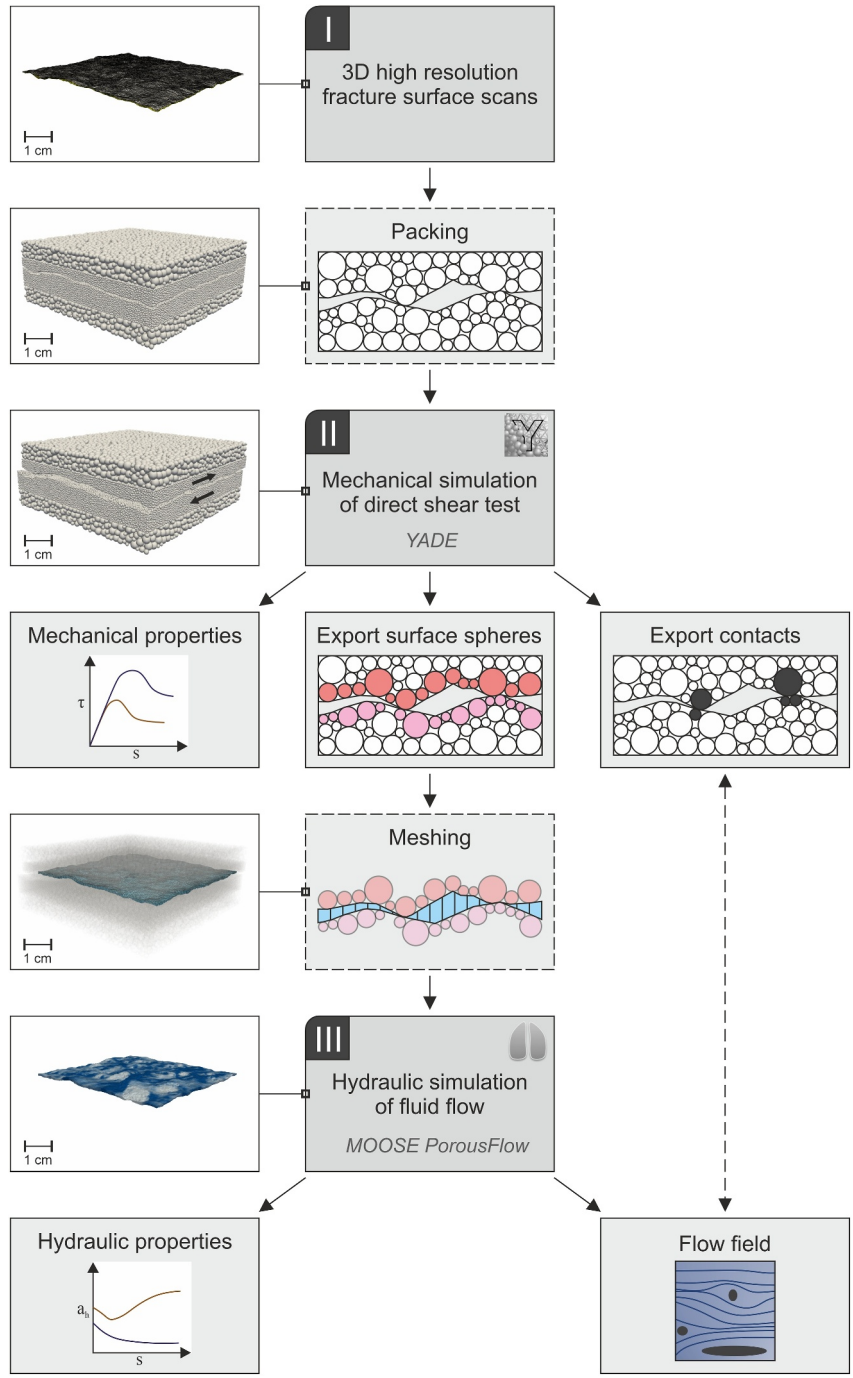

Figure 1. Workflow of the study with (I) the sample preparation from 3D fracture surface scans, (II) mechanical simulation of direct shear tests with a discrete element model, and (III) hydraulic simulation of fluid flow with a finite element model.

2.2. Mechanical Simulation of Direct Shear Tests

To simulate DST on the Flechtinger sandstone, we utilized the bonded particle model (BPM) proposed by Scholtès and Donzé (2013) implemented in the YADE software (Smilauer et al., 2021). First, the calibration of the BPM was required so that its mechanical properties match those of the Flechtinger sandstone. For this purpose, three standard rock experiments were conducted: (a) tensile, (b) uniaxial compression, and (c) triaxial compression tests. Subsequently, following the procedure proposed by Scholtès and Donzé (2013), the rock tests

were simulated on cylindrical samples, and the interparticle parameters of the BPM adjusted to match the experimental behavior of the Flechtinger sandstone (Table S2 in Supporting Information S1).

After the calibration, two blocks packed with spherical particles were generated using the two fracture surface scans. To limit the computational cost, each block was packed with two layers of particles (Figure 1). The particles of the inner layer have an average diameter of 400 μm, reproducing the actual grain size of the sandstone (100–500 μm) to represent the fracture surface roughness. The particles of the outer layers have an average diameter of 800 μm. The ratio of the maximum to minimum particle diameters in each layer is equal to 3.

After creating the packings, the DST simulations were performed. Each test consists of two phases: (a) the normal loading phase, in which an increasing load is applied perpendicularly onto the fracture plane until the predefined normal stress is reached, and (b) the shearing phase, in which the upper fracture block is displaced at a constant velocity parallel to the fracture plane while keeping the normal stress constant and the lower block fixed. To investigate the influence of normal stress on permeability, DST simulations were conducted at six different normal stresses: 1.5 MPa, 3.0 MPa, 4.0 MPa, 4.5 MPa, 7.5 MPa, and 15.0 MPa. For all simulations, the loading rates were chosen to ensure a quasi-static response of the model (i.e., the simulated behaviors are rate-independent).

2.3. Hydraulic Simulation

An extension of the YADE code was developed to combine the mechanical DST simulations with hydraulic flow simulations performed with the MOOSE framework (Giudicelli et al., 2024), and the built-in PorousFlow module, which allows finite element method (FEM) simulations of flow in porous and fractured media (Wilkins et al., 2020, 2021). Since the flow simulations require a finite element mesh, the fracture surface geometry was reconstructed from the BPM. In particular, the particles forming the fracture surfaces were traced throughout the simulations so that the evolving fracture surfaces could be rebuilt at any time of the DST (every 70 μm of shear displacement here). An automatized triangulation algorithm was used to interpolate the surfaces from the particles. Then, these surfaces were used to produce a hexahedral mesh representing the fracture flow domain (Figure 1). It should be noted that while the detached particles (gouge) are considered in the mechanical DEM model, they were assumed to be flushed out of the fracture in the hydraulic FEM model due to the numerical representation. Thus, the permeability values computed in the presence of gouge material should be regarded as an upper limit since only the particles forming the fracture walls were considered when building the FEM mesh for flow simulations.

The mesh consists of elements with an average size of 400 μm × 400 μm, similar to the average particle size. The flow in the rock matrix was neglected, given its low permeability of 0.1–1 mD (Cheng et al., 2020; Hassanzadegan et al., 2012).

To simulate fracture flow within MOOSE, a constant hydraulic pressure gradient was applied along the fracture length. To ensure laminar flow conditions required for the application of Darcy's law, a pressure difference of 0.1 Pa was applied between the inlet and the outlet of the fracture (Zimmerman & Bodvarsson, 1996). Since the influence of flow direction was also examined in this study, flow was either applied parallel or perpendicular to the shear direction.

Once steady-state conditions were reached, the permeability was calculated using Darcy's law (Cheng et al., 2020; Zimmerman & Bodvarsson, 1996):

$$k = \frac{\mu \bar{v} L}{\Delta p} \tag{1}$$

where k is the permeability of the fracture [m^2], μ is the dynamic viscosity of the fluid [Pa · s], $\bar{v}$ is the geometric mean of the flow velocity in the fracture [m/s], L is the length of the fracture domain [m] and Δp is the fluid pressure difference between inlet and outlet of the fracture [Pa].

3. Results and Discussion

Based on the DST simulations results (c.f. Text S3 and S4 in Supporting Information S1 and Movie S2), three shear induced hydraulic regimes can be identified depending on the normal stress applied: (a) an opening regime,

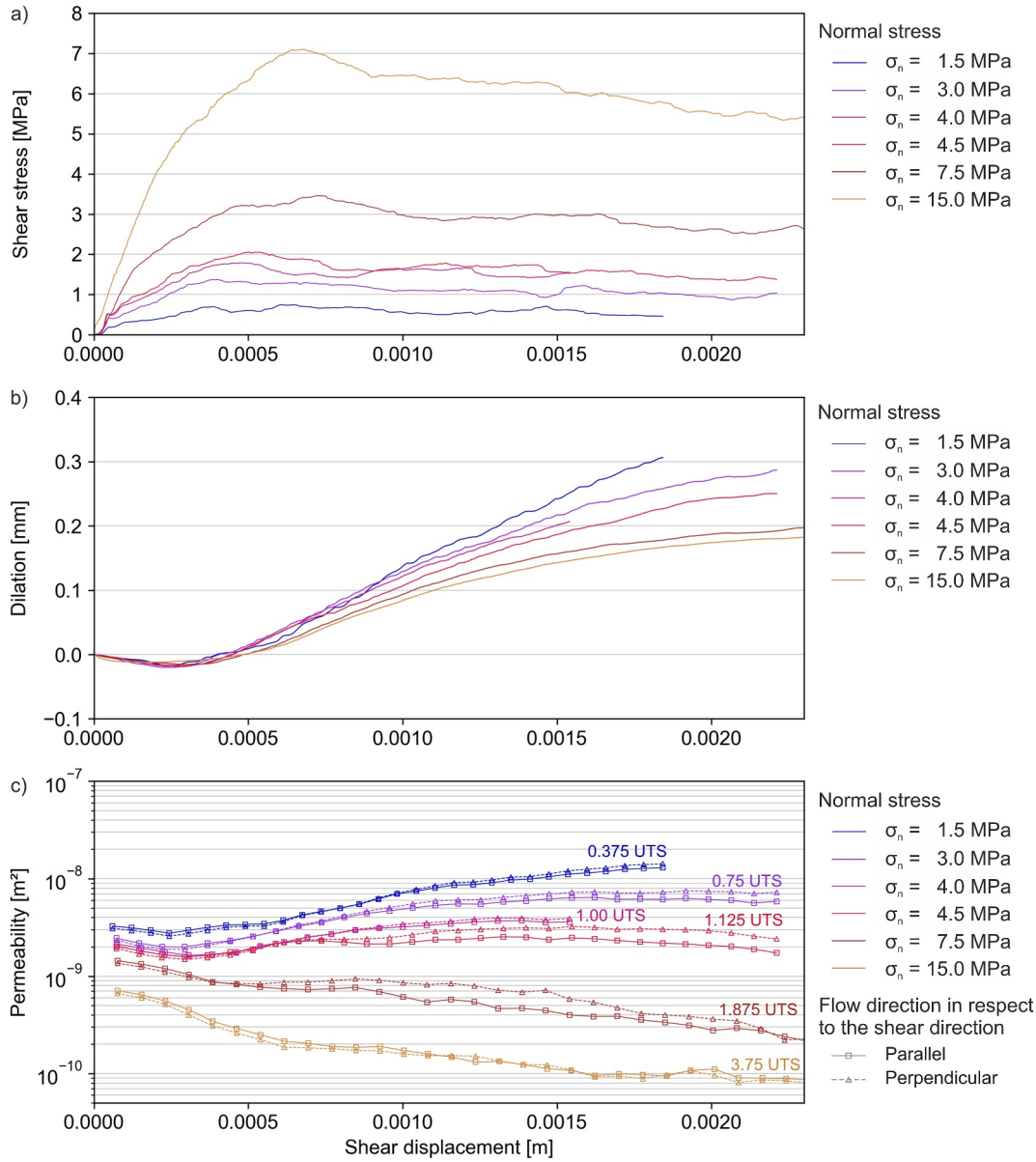

Figure 2. Shear displacement—(a) shear stress evolution, (b) dilation, and (c) permeability evolution during the direct shear test for six normal stress scenarios: 1.5 MPa, 3.0 MPa, 4.0 MPa, 4.5 MPa, 7.5 MPa, and 15.0 MPa. If the normal stress exceeds the UTS (4.0 MPa), dilation and permeability are significantly decreased.

in which the fracture permeability is enhanced during shearing, (b) a transitional regime, in which permeability shifts from a regime of increase to one of reduction, and (c) a closing regime, in which permeability is reduced during shearing (Figure 2). In the following sections, each regime is discussed.

3.1. Opening Regime

The opening regime is observed for DST performed at low normal stresses (1.5 and 3.0 MPa). Mechanically, this regime is characterized by two main characteristics: (a) after the first peak shear stress is reached, strain softening is limited and the shear stress oscillates and reaches the peak shear stress several times (Figure 2a), and (b) the dilation rate is maximal compared to the higher normal stress cases (Figure 2b). The pronounced dilation and the oscillating shear stress around the peak value result from sliding over the fracture surface asperities that do not break during the shearing process as confirmed by the few amount of gouge formed (Figure 3).

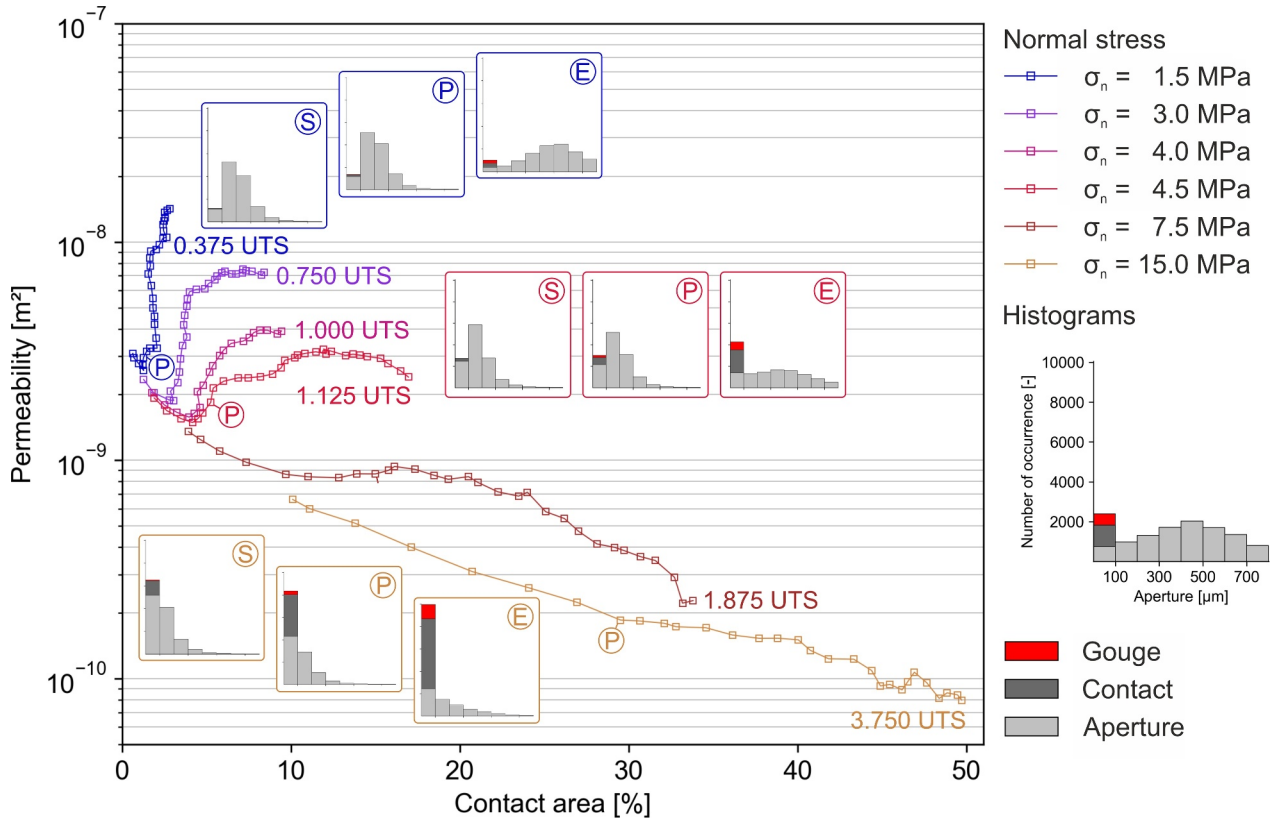

Figure 3. Permeability evolution (parallel to flow direction) and contact area during shearing with increasing normal stresses. Three curves are accompanied by three histograms showing the mechanical aperture distribution at the start (S), the peak shear stress (P), and the end (E) of each direct shear test. The color of the bars in the histogram indicates whether a cell in the hydraulic mesh is open (light gray), closed (dark gray), or would be filled with gouge (red).

As a result of ongoing dilation, the mode of the mechanical aperture distribution increases from 100 to 200 µm at the start to >400 µm at the end of the DST, as the distribution changes gradually from a log-normal to a Gaussian distribution. Additionally, an increase in mechanical apertures <100 µm as well as in contact area is observed with ongoing shear displacement. This shift in mechanical apertures has also been observed in μ-CT images of shear-induced fractures in shale (Welch et al., 2022). Since the investigated natural fracture has a small initial contact area (<2%), the displacement of the fracture results in an increase of contact area on the shear-facing sides of the asperities. Consequently, this leads to an enlargement of mechanical apertures on the shear-opposing side of asperities, increasing the overall mechanical aperture and creating potential flow channels (Figure 4a).

The hydraulic response reflects this mechanical behavior since the overall permeability of the fracture increases during the DST (Figure 2c). Additionally, flow channeling becomes increasingly pronounced with increasing shear displacement (Figures 4c–4f), which was also observed for flow through shear fractures in shales (Li et al., 2024; Welch et al., 2022).

Based on these observations, the following conclusions can be drawn: the fracture opens mainly due to mechanical dilation on intact asperities. Interestingly, the associated increase in contact area does not result in a reduction of permeability (Figure 3). This result is in contrast to previous findings showing that permeability tends to increase when contact area decreases during shearing (Barton et al., 1985; Chen et al., 2000).

3.2. Transitional Regime

At normal stresses >4.0 MPa, a transition from the above-described opening regime to a closing regime occurs (Figure 2c). The amount of gouge material and contact area increases significantly during shearing (Figure 3), leading to the closing of the main flow paths and to permeability reduction. Gouge material is formed from broken surface asperities (Gill et al., 2021). To characterize gouge formation, we analyzed the breaking modes of the

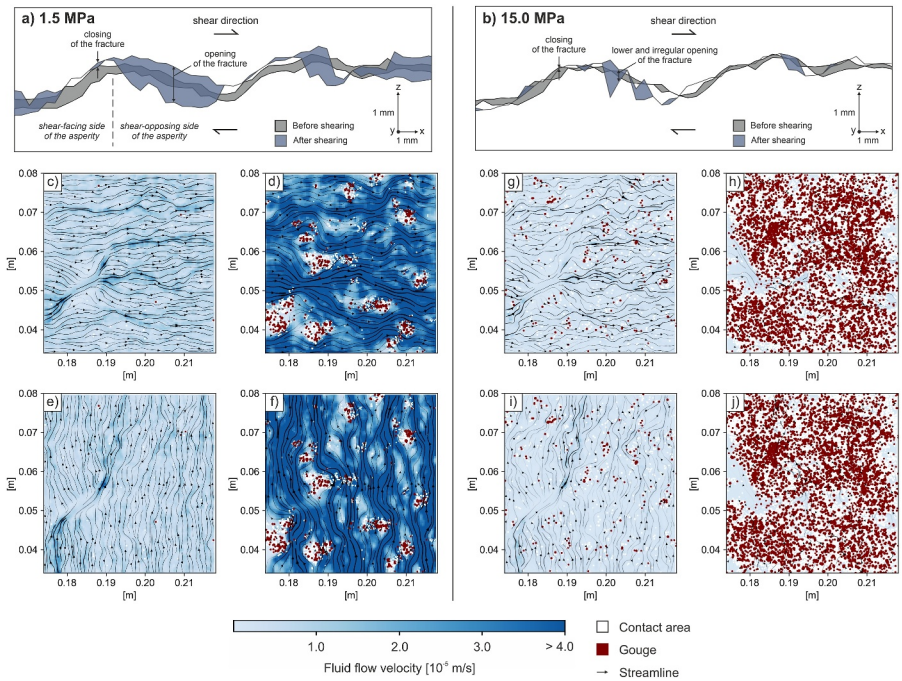

Figure 4. Results for normal stresses of 1.5 MPa (left) and 15.0 MPa (right). (a) and (b) Cross-section of the fracture before (gray) and after shearing (navy). (c–j) 2D flow fields with major streamlines (black arrows), contact area (white), and gouge (red) of the flow parallel to the shear direction before (c, g) and after shearing (d, h), as well as perpendicular to the shear direction before (e, i) and after shearing (f, j). The enlargement of major flow paths can be seen in (d) and (f). The hydraulic closing due to increasing contact areas and gouge is illustrated in (h) and (j).

bonds forming the BPM (Text S2 in Supporting Information S1) and observed that more than 99% of all cracks are tensile cracks (mode I) and only less than 1% of all cracks are shear cracks (mode II). This indicates that the breaking of fracture asperities is governed by shear-induced local tensile stresses. Remarkably, it is observed that the normal stress at which the permeability transitions from an increasing to a decreasing regime corresponds to the ultimate tensile strength (UTS) of the rock matrix (4.0 MPa). Previous studies have shown relationships between mechanical parameters and permeability (Deng et al., 2024; Gutierrez et al., 2000; Makurat et al., 1997; Milsch et al., 2016). Of particular interest are the studies by Makurat et al. (1997) and Gutierrez et al. (2000), which pointed out that the hydraulic transition occurs when the effective normal stress exceeds the UCS of the rock matrix they tested (a shale). However, while their results clearly highlight the fact that fracture permeability drastically decreased during shearing for normal stresses higher than the UCS value, the transition from an opening to a closing hydraulic regime seemed to be reached at lower normal stresses when reanalyzing their data (approximately 2 MPa). Unfortunately, the authors did not report the UTS of the rock they tested, and, at this point, we can only acknowledge that further investigations are required to state a representative threshold value for the transitional regime.

The increase in contact area related to fracture surface damage lead to additional changes in hydraulic properties, specifically in terms of flow anisotropy. This occurs in the DST at 3.0 MPa normal stress, as well as for the DST at 4.5 and 7.5 MPa normal stresses (Figure 2c). Due to transpression in shear direction, the permeability anisotropy (PA) $k_{\perp}/k_{//}$ is >1.2 with a peak anisotropy of $k_{\perp}/k_{//} = 1.6$. Similar observations on PA during shearing were observed in previous experimental studies (Auradou et al., 2005; Yeo et al., 1998), performed on digital synthetic fracture models (Matsuki et al., 1999) or numerically (Auradou et al., 2005; Li et al., 2024). Besides, gouge material also has a decisive influence on permeability, since it reduces dilation or clogs major flow paths, and, therefore, reduces mechanical apertures in the fracture (Gill et al., 2021; Li et al., 2023). However, many studies, especially numerical studies, do not consider gouge formation (e.g., Egert et al., 2023; Welch et al., 2022).

3.3. Closing Regime

For normal stresses exceeding the transition threshold of 4.0–4.5 MPa, the fracture is governed hydraulically by a closing regime during shearing (Figure 2c). Mechanically, this regime is characterized by a distinct peak shear stress and strain softening toward a residual state (Figure 2a). This behavior can be explained by the formation of a large amount of gouge associated to an increase of contact area (Figure 4b). Up to 50% of the fracture is closed by gouge particles or contacts (Figure 3). This is also reflected in the mechanical aperture distribution. The initial log-normal distribution is shifted to a logarithmic distribution with the mode <100 μm (Figure 3). The fracture is not just closed on the shear-facing sides of asperities, but also, in contrast to the opening regime, on the shear-opposing side (Figure 4b). Due to high normal and shear stresses, tensile cracks form in and around these asperities, promoting damage in the surrounding rock matrix and therefore producing even more gouge particles (Liu et al., 2016).

Hydraulically, the breakage of asperities and the associated increase of contact area lead to a total mechanical closure of all major flow paths during the DST, leaving only secondary flow paths open (Figures 4g–4j), and limiting flow anisotropy (Figure 2c). This hydraulic closure of the fracture is, therefore, mainly due to fracture surface damage instead of the pure vertical compaction of two fracture surfaces, as previously observed by Li et al. (2024).

A crucial assumption of our BPM approach is that gouge material results from the detachment of the particles (either isolated or clustered in aggregates) forming the fracture walls and that these particles are unbreakable. Since the sample mainly consists of quartz grains, such an assumption is acceptable at normal stresses up to 15 MPa. Nonetheless, it should be noted that, depending on material properties or alteration processes, actual gouge particles may break under high-stress conditions or large shear displacements (Fang and Wu, 2022; Li et al., 2023), and may have a significant effect on fracture closure (Zhao, 2013).

4. Conclusions

In this study, the hydro-mechanical behavior of a single sandstone fracture subjected to direct shear tests was investigated for normal stresses ranging from 1.5 to 15.0 MPa. A combined numerical approach (DEM and FEM) was designed to characterize fracture permeability changes during shearing. Our results indicate that three normal stress-related hydraulic regimes can be distinguished: (a) an opening regime at normal stresses between 1.5 and 3.0 MPa, (b) a transitional regime at around 4.0–4.5 MPa, and (c) a closing regime for normal stresses >4.5 MPa. These regimes can be characterized as follows:

1. In the opening regime, dilation on intact asperities governs the fracture behavior, and gouge and contact area formation are negligible. In this regime, permeability increases with increasing shear displacement since existing flow paths are enlarged.
2. In the transitional regime, increasing gouge formation and contact area start to affect the flow behavior of the fracture. This leads to high flow anisotropy, since gouge particles aggregate parallel to the shear direction and clog the flow in this direction, whereas perpendicular flow paths are kept open.
3. In the closing regime, significant asperity breakages form large amounts of gouge and contacts between the fracture surfaces. This results in less but still significant dilation on gouge particles. Hydraulically, existing flow paths close, and permeability is reduced.

Conclusively, all three regimes can occur in deep reservoirs depending on the rock material properties and in situ stress levels. For instance, according to our study, the transition to a closing regime would correspond to a depth of around 300 m for Flechtinger sandstone. Assuming long-term permeability enhancement after hydraulic stimulation should therefore be scrutinized in the context of geothermal projects realized in greater depths and stresses, since the lack of permeability can lead to shear-slip events and induced seismicity (Gaucher et al., 2015), as observed in Strasbourg in 2019/2020 (Schmittbuhl et al., 2022) and in Pohang in 2017 (Li et al., 2024). Nonetheless, it should be noted that these findings are based on a small-scale fracture and numerical simulations. To address this important limitation, future studies should aim for experimental validation of the present findings. Extrapolations to geothermal systems should also consider scale effects, fracture network connectivity and orientation. Furthermore, more sophisticated numerical models and larger-scale experiments are necessary on reservoir scale. Thus, further studies should focus on two key aspects: First, detailed small-scale hydro-mechanical models should be established to enable an exact representation of governing processes, especially

gouge formation, on the HM behavior during shearing. Second, methods should be developed to upscale small-scale results to reservoir scale. This includes the validation of such methods using laboratory and large in situ experiments in underground research laboratories.

Conflict of Interest

The authors declare no conflicts of interest relevant to this study.

Data Availability Statement

The fracture surface scans as well as all python scripts used to conduct the workflow presented in this study can be accessed via a Zenodo repository from the link https://doi.org/10.5281/zenodo.15583985 (Fuchs et al., 2025), or by contacting the authors. The simulation software (YADE and MOOSE) used in this study is open source and publicly available as cited in the main text. Additional references from the appendix: (Duriez et al., 2016; Hart et al., 1988; Hassanzadegan et al., 2014; Vogler et al., 2018).

Acknowledgments

The authors thank Christian Kluge and Liang Pei for conducting the rock tests for model calibration. Marco Fuchs was supported by the Karlsruhe House of Young Scientists (KHYS) and the InVolc Graduate Track of the Université Clermont Auvergne. This work benefited from the French government initiative "programme d'investissements d'avenir" managed by the Agence Nationale de la Recherche (ANR) under grant ANR-20-SFRI-0003 project CAP GS. The authors would like to acknowledge the constructive comments made by the two reviewers, which helped to improve this manuscript. Open Access funding enabled and organized by Projekt DEAL.

References

Amann, F., Gischig, V., Evans, K., Doetsch, J., Jalali, R., Valley, B., et al. (2018). The seismo-hydromechanical behavior during deep geothermal reservoir stimulations: Open questions tackled in a decameter-scale in situ stimulation experiment. *Solid Earth*, *9*(1), 115–137. https://doi.org/10.5194/se-9-115-2018

Asadi, M. S., Rasouli, V., & Barla, G. (2012). A bonded particle model simulation of shear strength and asperity degradation for rough rock fractures. *Rock Mechanics and Rock Engineering*. https://doi.org/10.1007/s00603-012-0231-4

Auradou, H. (2009). Influence of wall roughness on the geometrical, mechanical and transport properties of single fractures. *Journal of Physics D Applied Physics*, *42*(21), 214015. https://doi.org/10.1088/0022-3727/42/21/214015

Auradou, H., Drazer, G., Hulin, J. P., & Koplik, J. (2005). Permeability anisotropy induced by the shear displacement of rough fracture walls. *Water Resources Research*, *41*(9), 2005WR003938. https://doi.org/10.1029/2005WR003938

Barton, N. (1982). *Modelling rock joint behavior form in situ block tests: Implications for nuclear waste repository design: Technical report*. Office of Nuclear Waste Isolation, Battelle Project Mangement Division, Columbus.

Barton, N., Bandis, S., & Bakhtar, K. (1985). Strength, deformation and conductivity coupling of rock joints. *International Journal of Rock Mechanics and Mining Sciences & Geomechanics Abstracts*, *22*(3), 121–140. https://doi.org/10.1016/0148-9062(85)93227-9

Barton, N., & De Quadros, E. F. (1997). Joint aperture and roughness in the prediction of flow and groutability of rock masses. *International Journal of Rock Mechanics and Mining Sciences*, *34*(3–4), 252.e1–252.e14. https://doi.org/10.1016/S1365-1609(97)00081-6

Blöcher, G., Kluge, C., Milsch, H., Cacace, M., Jacquey, A. B., & Schmittbuhl, J. (2019). Permeability of matrix-fracture systems under mechanical loading – Constraints from laboratory experiments and 3-D numerical modelling. *Advances in Geosciences*, *49*, 95–104. https://doi.org/10.5194/adgeo-49-95-2019

Cardona, A., Finkbeiner, T., & Santamarina, J. C. (2021). Natural rock fractures: From aperture to fluid flow. *Rock Mechanics and Rock Engineering*, *54*(11), 5827–5844. https://doi.org/10.1007/s00603-021-02565-1

Carey, J. W., Lei, Z., Rougier, E., Mori, H., & Viswanathan, H. (2015). Fracture-permeability behavior of shale. *Journal of Unconventional Oil and Gas Resources*, *11*, 27–43. https://doi.org/10.1016/j.juogr.2015.04.003

Chen, Y., Liang, W., Selvadurai, A. P. S., & Zhao, Z. (2021). Influence of asperity degradation and gouge formation on flow during rock fracture shearing. *International Journal of Rock Mechanics and Mining Sciences*, *143*, 104795. https://doi.org/10.1016/j.ijrmms.2021.104795

Chen, Z., Narayan, S. P., Yang, Z., & Rahman, S. S. (2000). An experimental investigation of hydraulic behaviour of fractures and joints in granitic rock. *International Journal of Rock Mechanics and Mining Sciences*, *37*(7), 1061–1071. https://doi.org/10.1016/S1365-1609(00)00039-3

Cheng, C., Hale, S., Milsch, H., & Blum, P. (2020). Measuring hydraulic fracture apertures: A comparison of methods. *Solid Earth*, *11*(6), 2411–2423. https://doi.org/10.5194/se-11-2411-2020

Deng, Q., Schmittbuhl, J., Cacace, M., & Blöcher, G. (2024). Mechanical stiffness and permeability of a reservoir-scale rough fracture during closure. *JGR Solid Earth*, *129*(9), e2024JB029001. https://doi.org/10.1029/2024JB029001

Duriez, J., Scholtès, L., & Donzé, F.-V. (2016). Micromechanics of wing crack propagation for different flaw properties. *Engineering Fracture Mechanics*, *153*, 378–398. https://doi.org/10.1016/j.engfracmech.2015.12.034

Egert, R., Nitschke, F., Gholami Korzani, M., & Kohl, T. (2023). Spatial characterization of channeling in sheared rough-walled fractures in the transition to nonlinear fluid flow. *Water Resources Research*, *59*(10), e2022WR034362. https://doi.org/10.1029/2022WR034362

Ellsworth, W. L. (2013). Injection-induced earthquakes. *Science*, *341*(6142), 1225942. https://doi.org/10.1126/science.1225942

Esaki, T., Du, S., Mitani, Y., Ikusada, K., & Jing, L. (1999). Development of a shear-flow test apparatus and determination of coupled properties for a single rock joint. *International Journal of Rock Mechanics and Mining Sciences*, *36*(5), 641–650. https://doi.org/10.1016/S0148-9062(99)00044-3

Fang, Y., Elsworth, D., Wang, C., Ishibashi, T., & Fitts, J. P. (2017). Frictional stability-permeability relationships for fractures in shales. *JGR Solid Earth*, *122*(3), 1760–1776. https://doi.org/10.1002/2016JB013435

Fang, Z., & Wu, W. (2022). Laboratory friction-permeability response of rock fractures: A review and new insights. *Geomech Geophys Geo-energ Geo-resour*, *8*(1), 15. https://doi.org/10.1007/s40948-021-00316-8

Fischer, C., Dunkl, I., Von Eynatten, H., Wijbrans, J. R., & Gaupp, R. (2012). Products and timing of diagenetic processes in upper rotliegend sandstones from bebertal (North German Basin, Parchim formation, flechtingen high, Germany). *Geological Magazine*, *149*(5), 827–840. https://doi.org/10.1017/S0016756811001087

Frash, L. P., Carey, J. W., Lei, Z., Rougier, E., Ickes, T., & Viswanathan, H. S. (2016). High-stress triaxial direct-shear fracturing of utica shale and in situ X-ray microtomography with permeability measurement. *JGR Solid Earth*, *121*(7), 5493–5508. https://doi.org/10.1002/2016JB012850

Fuchs, M., Blum, P., Blöcher, G., & Scholtès, L. (2025). Data and software supporting "Permeability evolution and gouge formation during fracture shearing" [Dataset]. *Zenodo*. https://doi.org/10.5281/zenodo.15583985

Fuchs, M., Hale, S., Blesch, L., Rau, G. C., Menberg, K., & Blum, P. (2024). Evaluating fracture surface imaging methods using flow simulations and air permeameter measurements. *Rock Mechanics and Rock Engineering*, *57*(3), 1849–1860. https://doi.org/10.1007/s00603-023-03615-6

Fuchs, M., Suzuki, A., Hasumi, T., & Blum, P. (2024). Investigating rough single-fracture permeabilities with persistent homology. *Solid Earth*, *15*(3), 353–365. https://doi.org/10.5194/se-15-353-2024

Gaucher, E., Schoenball, M., Heidbach, O., Zang, A., Fokker, P. A., van Wees, J. D., & Kohl, T. (2015). Induced seismicity in geothermal reservoirs: Physical processes and key parameters. In *World geothermal congress*, (pp. 1–13).

Gill, M., Crandall, D., Moore, J., Mackey, P., & Brown, S. (2021). Gouge formation and dilation impacts to flow during fracture shearing. *International Journal of Rock Mechanics and Mining Sciences*, *147*, 104920. https://doi.org/10.1016/j.ijrmms.2021.104920

Giudicelli, G., Lindsay, A., Harbour, L., Icenhour, C., Li, M., Hansel, J. E., et al. (2024). 3.0 - MOOSE: Enabling massively parallel multiphysics simulations. *SoftwareX*, *26*, 101690. https://doi.org/10.1016/j.softx.2024.101690

Gutierrez, M., Øino, L. E., & Nygård, R. (2000). Stress-dependent permeability of a de-mineralised fracture in shale. *Marine and Petroleum Geology*, *17*(8), 895–907. https://doi.org/10.1016/S0264-8172(00)00027-1

Gutjahr, T., Hale, S., Keller, K., Blum, P., & Winter, S. (2022). Quantification of fracture roughness by change probabilities and hurst exponents. *Mathematical Geosciences*, *54*(4), 679–710. https://doi.org/10.1007/s11004-021-09985-3

Hale, S., & Blum, P. (2022). Bestimmung der hydraulischen Durchlässigkeiten eines Sandsteins mithilfe eines Luftpermeameters. *Grundwasser - Zeitschrift der Fachsektion Hydrogeologie*, *27*(1), 57–65. https://doi.org/10.1007/s00767-021-00504-z

Hale, S., Naab, C., Butscher, C., & Blum, P. (2020). Method comparison to determine hydraulic apertures of natural fractures. *Rock Mechanics and Rock Engineering*, *53*(3), 1467–1476. https://doi.org/10.1007/s00603-019-01966-7

Hart, R., Cundall, P. A., & Lemos, J. (1988). Formulation of a three-dimensional distinct element model—Part II. Mechanical calculations for motion and interaction of a system composed of many polyhedral blocks. *International Journal of Rock Mechanics and Mining Sciences & Geomechanics Abstracts*, *25*(3), 117–125. https://doi.org/10.1016/0148-9062(88)92294-2

Hassanzadegan, A., Blöcher, G., Milsch, H., Urpi, L., & Zimmermann, G. (2014). The effects of temperature and pressure on the porosity evolution of flechtinger sandstone. *Rock Mechanics and Rock Engineering*, *47*(2), 421–434. https://doi.org/10.1007/s00603-013-0401-z

Hassanzadegan, A., Blöcher, G., Zimmermann, G., & Milsch, H. (2012). Thermoporoelastic properties of flechtinger sandstone. *International Journal of Rock Mechanics and Mining Sciences*, *49*, 94–104. https://doi.org/10.1016/j.ijrmms.2011.11.002

Heidsiek, M., Butscher, C., Blum, P., & Fischer, C. (2020). Small-scale diagenetic facies heterogeneity controls porosity and permeability pattern in reservoir sandstones. *Environmental Earth Sciences*, *79*(18), 425. https://doi.org/10.1007/s12665-020-09168-z

Heiland, J. (2003). Permeability of triaxially compressed sandstone: Influence of deformation and strain-rate on permeability. In H.-J. Kümpel (Ed.), *Thermo-hydro-mechanical coupling in fractured rock* (pp. 889–908). Birkhäuser Basel.

Kluge, C., Blöcher, G., Barnhoorn, A., Schmittbuhl, J., & Bruhn, D. (2021). Permeability evolution during shear zone initiation in low-porosity rocks. *Rock Mechanics and Rock Engineering*, *54*(10), 5221–5244. https://doi.org/10.1007/s00603-020-02356-0

Lambert, C., & Coll, C. (2014). Discrete modeling of rock joints with a smooth-joint contact model. *Journal of Rock Mechanics and Geotechnical Engineering*, *6*, 1–12. https://doi.org/10.1016/j.jrmge.2013.12.003

Li, X., Zhang, F., Xiu, N., Weng, D., Cai, B., & Fu, H. (2024). Shear-induced permeability evolution of natural fractures in granite: Implications for stimulation of EGS reservoirs. *Engineering Geology*, *338*, 107629. https://doi.org/10.1016/j.enggeo.2024.107629

Li, Z., Ma, X., Kong, X.-Z., Saar, M. O., & Vogler, D. (2023). Permeability evolution during pressure-controlled shear slip in saw-cut and natural granite fractures. *Rock Mechanics Bulletin*, *2*, 100027. https://doi.org/10.1016/j.rockmb.2022.100027

Liu, H. Y., Han, H., An, H. M., & Shi, J. J. (2016). Hybrid finite-discrete element modelling of asperity degradation and gouge grinding during direct shearing of rough rock joints. *Int J Coal Sci Technol*, *3*, 295–310. https://doi.org/10.1007/s40789-016-0142-1

Louis, C. (1969). *A study of groundwater flow in jointed rock and its influence on the stability of rock masses*. Imperial College of Science and Technology.

Makurat, A., Gutierrez, M., & Backer, L. (1997). Fracture flow and fracture cross flow experiments. In *Norwegian petroleum society special publications* (pp. 139–148). Elsevier.

Matsuki, K., Lee, J.-J., Sakaguchi, K., & Hayashi, K. (1999). Size effect in flow conductance of a closed small-scale hydraulic fracture in granite. *Geothermal Science and Technology*, *1–4*, 113–138.

Milsch, H., Hofmann, H., & Blöcher, G. (2016). An experimental and numerical evaluation of continuous fracture permeability measurements during effective pressure cycles. *International Journal of Rock Mechanics and Mining Sciences*, *89*, 109–115. https://doi.org/10.1016/j.ijrmms.2016.09.002

Nguyen, H. N. G., Scholtès, L., Guglielmi, Y., Donzé, F. V., Ouraga, Z., & Souley, M. (2021). Micromechanics of sheared granular layers activated by fluid pressurization. *Geophysical Research Letters*, *48*(14), e2021GL093222. https://doi.org/10.1029/2021GL093222

Olsson, R., & Barton, N. (2001). An improved model for hydromechanical coupling during shearing of rock joints. *International Journal of Rock Mechanics and Mining Sciences*, *38*(3), 317–329. https://doi.org/10.1016/S1365-1609(00)00079-4

Renshaw, C. E. (1995). On the relationship between mechanical and hydraulic apertures in rough-walled fractures. *Journal of Geophysical Research*, *100*(B12), 24629–24636. https://doi.org/10.1029/95JB02159

Schmittbuhl, J., Lambotte, S., Lengliné, O., Grunberg, M., Jund, H., Vergne, J., et al. (2022). Induced and triggered seismicity below the city of Strasbourg, France from November 2019 to January 2021. *Comptes Rendus Geoscience*, *353*, 561–584. https://doi.org/10.5802/crgeos.71

Scholtès, L., & Donzé, F.-V. (2013). A DEM model for soft and hard rocks: Role of grain interlocking on strength. *Journal of the Mechanics and Physics of Solids*, *61*(2), 352–369. https://doi.org/10.1016/j.jmps.2012.10.005

Smilauer, V., Angelidakis, V., Catalano, E., Caulk, R., Chareyre, B., Chevremont, W., et al. (2021). Yade documentation.

Tatone, B. S. A., & Grasselli, G. (2015). Characterization of the effect of normal load on the discontinuity morphology in direct shear specimens using X-ray micro-CT. *Acta Geotech*, *10*(1), 31–54. https://doi.org/10.1007/s11440-014-0320-5

Vogler, D., Settgast, R. R., Annavarapu, C., Madonna, C., Bayer, P., & Amann, F. (2018). Experiments and simulations of fully hydro-mechanically coupled response of rough fractures exposed to high-pressure fluid injection. *Journal of Geophysical Research: Solid Earth*, *123*(2), 1186–1200. https://doi.org/10.1002/2017JB015057

Walsh, J. B. (1981). Effect of pore pressure and confining pressure on fracture permeability. *International Journal of Rock Mechanics and Mining Sciences & Geomechanics Abstracts*, *18*(5), 429–435. https://doi.org/10.1016/0148-9062(81)90006-1

Wang, C., Elsworth, D., & Fang, Y. (2019). Ensemble shear strength, stability, and permeability of mixed mineralogy fault gouge recovered from 3D granular models. *JGR Solid Earth*, *124*(1), 425–441. https://doi.org/10.1029/2018JB016066

Wang, C., Elsworth, D., Fang, Y., & Zhang, F. (2020). Influence of fracture roughness on shear strength, slip stability and permeability: A mechanistic analysis by three-dimensional digital rock modeling. *Journal of Rock Mechanics and Geotechnical Engineering*, *12*(4), 720–731. https://doi.org/10.1016/j.jrmge.2019.12.010

Welch, N. J., Carey, J. W., Frash, L. P., Hyman, J. D., Hicks, W., Meng, M., et al. (2022). Effect of shear displacement and stress changes on fracture hydraulic aperture and flow anisotropy. *Transport in Porous Media*, *141*(1), 17–47. https://doi.org/10.1007/s11242-021-01708-w

Wenning, Q. C., Madonna, C., Kurotori, T., & Pini, R. (2019). Spatial mapping of fracture aperture changes with shear displacement using x-ray computerized tomography. *JGR Solid Earth*, *124*(7), 7320–7340. https://doi.org/10.1029/2019JB017301

Wilkins, A., Green, C., & Ennis-King, J. (2020). PorousFlow: A multiphysics simulation code for coupled problems in porous media. *JOSS*, *5*(55), 2176. https://doi.org/10.21105/joss.02176

Wilkins, A., Green, C. P., & Ennis-King, J. (2021). An open-source multiphysics simulation code for coupled problems in porous media. *Computers & Geosciences*, *154*, 104820. https://doi.org/10.1016/j.cageo.2021.104820

Witherspoon, P. A., Wang, J. S. Y., Iwai, K., & Gale, J. E. (1980). Validity of cubic law for fluid flow in a deformable rock fracture. *Water Resources Research*, *16*(6), 1016–1024. https://doi.org/10.1029/WR016i006p01016

Yeo, I. W., De Freitas, M. H., & Zimmerman, R. W. (1998). Effect of shear displacement on the aperture and permeability of a rock fracture. *International Journal of Rock Mechanics and Mining Sciences*, *35*(8), 1051–1070. https://doi.org/10.1016/S0148-9062(98)00165-X

Zhao, Z. (2013). Gouge particle evolution in a rock fracture undergoing shear: A microscopic DEM study. *Rock Mechanics and Rock Engineering*, *46*(6), 1461–1479. https://doi.org/10.1007/s00603-013-0373-z

Zimmerman, R. W., & Bodvarsson, G. S. (1996). Hydraulic conductivity of rock fractures. *Transport in Porous Media*, *23*(1). https://doi.org/10.1007/BF00145263

Zimmermann, G., Moeck, I., & Blöcher, G. (2010). Cyclic waterfrac stimulation to develop an enhanced geothermal system (EGS)—Conceptual design and experimental results. *Geothermics*, *39*(1), 59–69. https://doi.org/10.1016/j.geothermics.2009.10.003